NK cells converge lytic granules to promote cytotoxicity and prevent bystander killing

Hsiang-Ting Hsu,[1,2] Emily M. Mace,[1,2] Alexandre F. Carisey,[1,2] Dixita I. Viswanath,[1,3] Athanasia E. Christakou,[4] Martin Wiklund,[4] Björn Önfelt,[4,5] and Jordan S. Orange[1,2,3]

[1]Center for Human Immunobiology, Texas Children's Hospital, Houston, TX 77030
[2]Department of Pediatrics, Pathology and Immunology, Baylor College of Medicine, Houston, TX 77030
[3]Rice University, Houston, TX 77005
[4]Department of Applied Physics, KTH Royal Institute of Technology, 106 91 Stockholm, Sweden
[5]Department of Microbiology, Tumor and Cell Biology, Karolinska Institute, 171 77 Stockholm, Sweden

Natural killer (NK) cell activation triggers sequential cellular events leading to destruction of diseased cells. We previously identified lytic granule convergence, a dynein- and integrin signal–dependent movement of lysosome-related organelles to the microtubule-organizing center, as an early step in the cell biological process underlying NK cell cytotoxicity. Why lytic granules converge during NK cell cytotoxicity, however, remains unclear. We experimentally controlled the availability of human ligands to regulate NK cell signaling and promote granule convergence with either directed or nondirected degranulation. By the use of acoustic trap microscopy, we generated specific effector–target cell arrangements to define the impact of the two modes of degranulation. NK cells with converged granules had greater targeted and less nonspecific "bystander" killing. Additionally, NK cells in which dynein was inhibited or integrin blocked under physiological conditions demonstrated increased nondirected degranulation and bystander killing. Thus, NK cells converge lytic granules and thereby improve the efficiency of targeted killing and prevent collateral damage to neighboring healthy cells.

Introduction

Natural killer (NK) cells are cytotoxic lymphocytes that play a critical role in the elimination of transformed and virally infected cells (Vivier et al., 2008). NK cells express numerous germline-encoded activating receptors including the natural cytotoxicity receptors, CD16 (IgG Fc receptor), and adhesion receptors such as the integrin LFA-1(Lanier, 2005). The activating receptors recognize signatures of cell stress or disease, including IgG opsonization via CD16, to promote signaling pathways. These pathways, when surpassing critical thresholds, initiate a stepwise series of cellular events that can result in secretion of specialized secretory lysosomes termed "lytic granules" (Mace et al., 2014). After adhering to a prototypical target cell, NK cells rapidly reorient their lytic granules to the microtubule-organizing center (MTOC) using dynein motors (Mentlik et al., 2010; James et al., 2013; Zhang et al., 2014; Ham et al., 2015). This is followed by polarization of the lytic granules and MTOC to the interface formed with the target cell (also known as the lytic immunological synapse; Katz et al., 1982; Laan et al., 2012; Yi et al., 2013) and then degranulation (Liu et al., 2011), which facilitates fatal secretion of the pore-forming molecule perforin and lytic enzymes onto the target cell.

Among cells that contain lysosome-related organelles, NK cells and cytotoxic T lymphocytes (CTLs) are the only ones known to converge their granules before secreting the granule contents onto target cells (Mentlik et al., 2010; Ritter et al., 2015). Granule convergence in NK cells can be triggered by the integrin LFA-1 as well as by other activation receptors and precedes any commitment to cytotoxicity. The dynein-dependent minus end–directed movement of lytic granules is dependent on Src family kinase activity as well as signaling downstream of LFA-1 signaling (James et al., 2013; Zhang et al., 2014) but is independent of actin and microtubule reorganization and other signals required for cytotoxicity (Mentlik et al., 2010; James et al., 2013).

In comparison to lymphocytes, mast cells and melanocytes undergo multidirectional dispersion of secretory organelles (Marks et al., 2013), presumably allowing for efficient distribution of their granule contents. In these cells, convergence prevents (not promotes) degranulation (Nascimento et al., 2003). The early, rapid, and regulated convergence of lytic

Correspondence to Jordan S. Orange: orange@bcm.edu

Abbreviations used: ADCC, antibody-dependent cell-mediated cytotoxicity; CTL, cytotoxic T lymphocyte; eNK, ex vivo NK cells; ICAM-1, intercellular adhesion molecule 1; IS, immunological synapse; MTOC, microtubule organizing center; NK, natural killer; RTX, rituximab; UGATm, ultrasound-guided acoustic-trap microscopy.

The Rockefeller University Press $30.00
J. Cell Biol. Vol. 215 No. 6 875–889
https://doi.org/10.1083/jcb.201604136

granules in cytotoxic cells of both the innate (Mentlik et al., 2010) and adaptive (Ritter et al., 2015) arms of the immune system suggests it is an evolutionarily conserved mechanism. Any contribution of this mechanism to cytotoxicity, however, has not been identified or proven. We hypothesized that it was to increase efficiency of killing while minimizing bystander killing.

To potentially identify any utility to lytic granule convergence in NK cell cytotoxicity, we used approaches to regulate the balance of signaling through LFA-1 and CD16 to promote degranulation either without granule polarization or with both polarization and degranulation. We combined these with highly resolved four-dimensional confocal and ultrasound-guided acoustic-trap microscopy (UGATm) systems (Christakou et al., 2013) to create specific coordinated cell interactions and track lytic granules in live NK cells to correlate lytic granule positioning with target cell death. We demonstrate that NK cell lytic granule convergence improves the efficiency of targeted lytic granule secretion and prevents bystander killing.

Results

CD16 engagement induces conjugate formation and degranulation but not lytic granule convergence in NK cells

NK cells converge lytic granules upon recognition of target cells. Although the signals directing this process have been elucidated, it remains unclear why NK cells converge granules. To address this question, we used and modified a *Drosophila melanogaster* S2 target cell system. Because S2 cells are evolutionarily distant from mammalian cells, they do not express ligands recognized by human NK cells and are therefore inert (March et al., 2010). Expression of human intercellular adhesion molecule 1 (ICAM-1) on S2 cells ligates NK cell LFA-1 and causes lytic granule polarization without degranulation, whereas opsonization of the S2 cell with antiserum engages the IgG Fc receptor CD16 and promotes degranulation without granule/MTOC polarization (Bryceson et al., 2005). We first wanted to determine precise granule positioning after isolated triggering of either receptor to better understand potential directionality in granule targeting.

We used two different CD16-expressing clonal human NK cell lines (YTS and NK92), as they are effective in cytotoxicity but are amenable to in vitro manipulation, as well as ex vivo NK (eNK) cells, which more directly reflect actual human immunity. Of the cell lines, the lytic granule positioning in YTS cells is likely more reflective of eNK cells, because NK92 cells require growth in interleukin-2, which can independently alter granule positioning via Src signaling (James et al., 2013). In each type of NK cell, we measured the distance between every lytic granule and the MTOC (in the plane of the MTOC) in NK cells incubated with S2 cells, S2 cells expressing the ligand for LFA-1–ICAM-1 (S2-IC1), or S2 or S2-IC1 cells coated with S2 antiserum to trigger CD16 (S2 antiserum or S2-IC1 antiserum). Lytic granules in CD16-expressing YTS cells (YTS-CD16; Fig. 1, A and C), NK92 cells (NK92-CD16; Fig. S1, A and B), and eNK cells (Fig. 1, B and D) converged to the MTOC when conjugated with S2-IC1 or S2-IC1 antiserum cells. Lytic granules in NK cells incubated with S2 antiserum cells, however, were not significantly different in their distance from the MTOC compared with those incubated with control S2 cells or unconjugated NK cells (Figs. 1 and S1).

NK cell cytotoxicity consists of a stepwise series of tightly regulated cellular events that requires their contact with and adherence to target cells as an early step in the process (Mace et al., 2014). Although NK cells form conjugates with S2 cells coated with S2 antiserum (Fig. S2, A and B; Bryceson et al., 2005), we hypothesized that purified anti–S2-IgG should perform similarly while potentially increasing the specificity of the signal input for NK cells via CD16, because any other serum components would be removed. Thus, we developed an S2-specific IgG and used this to opsonize S2 or S2-IC1 cells (denoted as S2-IgG or S2-IC1-IgG), which were incubated with YTS-CD16, NK92-CD16, or eNK cells, for 0, 10, 30, and 60 min (unlabeled S2 or S2-IC1 cells were used as controls). CD16 engagement by anti–S2-IgG induced conjugate formation in YTS-CD16 (Fig. 2 A), NK92-CD16 (Fig. 2 B), and eNK (Fig. 2 C) cells, whereas conjugate formation with unlabeled S2 cells was negligible. In all NK cells tested, purified IgG allowed for conjugate efficiency comparable to that of antiserum.

To ensure that the purified anti-S2 antibodies trigger degranulation of the CD16-expressing NK cell lines and eNK cells, we quantified CD107a exposure on the NK cell surface using flow cytometry. YTS-CD16, NK92-CD16, or eNK cells mixed with S2, S2-IgG, S2-IC1, or S2-IC1-IgG cells demonstrated that engagement of CD16 induced degranulation. Addition of ICAM-1 further enhanced degranulation in the NK cell lines (Fig. 2, D and E; and Fig. S2 C), but not in eNK cells, which had similar CD107a levels when conjugated with S2-IgG or S2-IC1-IgG (Figs. 2 F and S2 C), as previously reported for antiserum-coated S2 cells (Bryceson et al., 2005). NK cells conjugated with S2 or S2-IC1 cells displayed negligible CD107a levels. Thus, purified anti–S2-IgG induced conjugate formation in the absence of ICAM-1 and triggered degranulation.

Convergence promotes lytic granule–directed secretion

Because isolated ligation of CD16 promotes degranulation despite granules being diffusely localized, we hypothesized that at least some degranulation would be nondirectional. Using imaging flow cytometry for high-throughput measurement of NK cell–target cell conjugates, we evaluated the positioning of degranulation relative to the immunological synapse (IS) in YTS-CD16 NK cells triggered with S2-IgG or S2-IC1-IgG (Fig. 3 A). The area, mean fluorescence intensity, and total fluorescence of lytic granules (denoted by LysoTracker red; Fig. 3 B) and degranulation (denoted by CD107a; Fig. 3 C) at the IS were significantly higher in YTS-CD16 cells conjugated with S2-IC1-IgG cells than in those conjugated with S2-IgG cells. The latter displayed both fewer synaptic granules and lower degranulation, suggesting nondirectionality despite the presence of an opsonized target cell.

To further define this process, we performed live-cell microscopy to track the lytic granule movements while identifying degranulation events using a stably expressed degranulation indicator fusion protein (LAMP1-pHluorin; Rak et al., 2011). Although LAMP1-pHluorin cannot be introduced into eNK cells without inducing their activation, we generated YTS-CD16 cells stably expressing LAMP1-pHluorin. In these cells, acidified granules can be tracked via LysoTracker red fluorescence, with their release marked by a transition to green fluorescence caused by granule de-acidification and pHluorin excitation. When

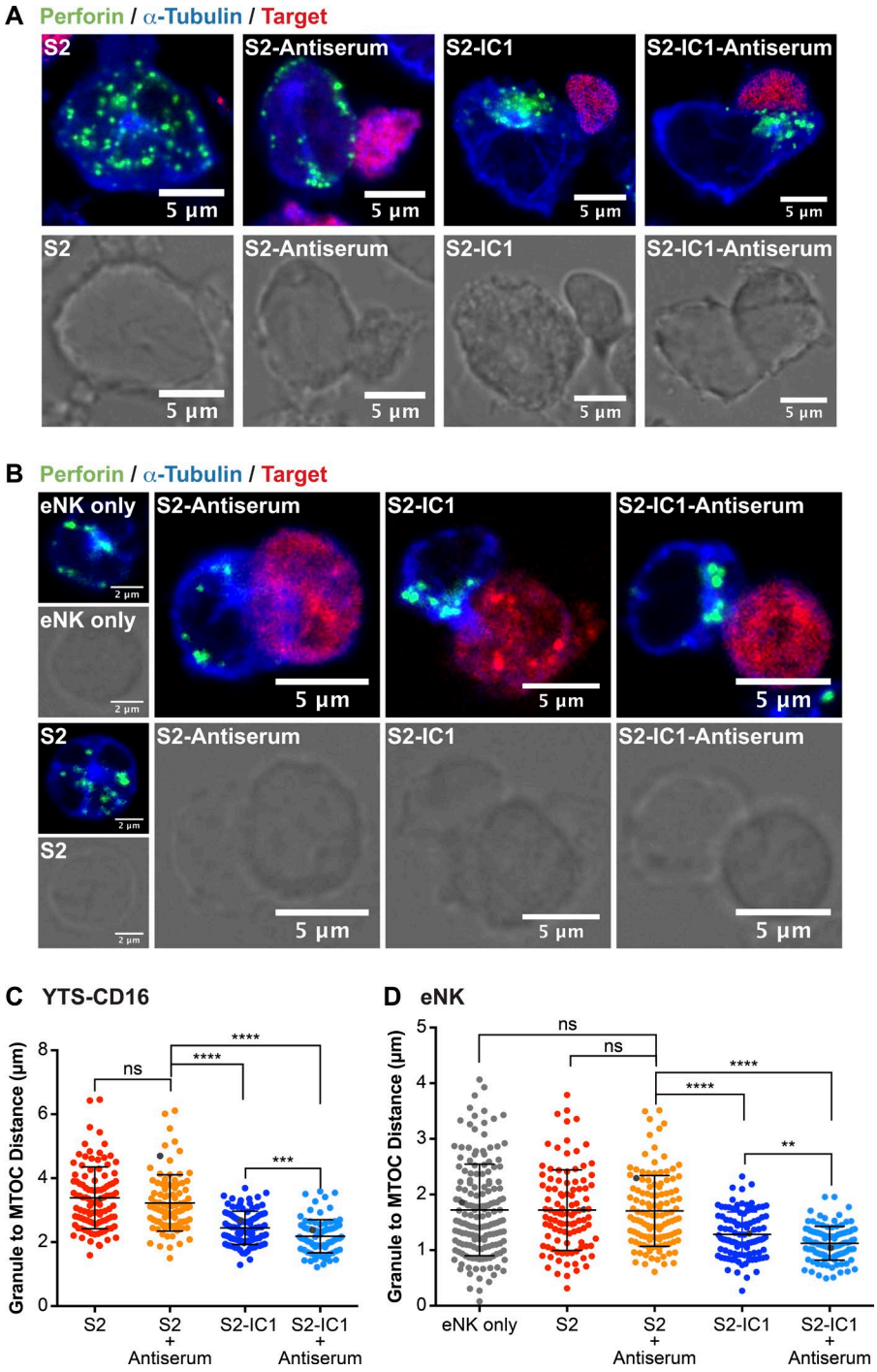

Figure 1. **LFA-1 but not CD16 engagement induces lytic granule convergence in NK cells.** Fixed-cell confocal microscopy of YTS-CD16 (A) and eNK (B) cells incubated with S2, S2 antiserum, S2-IC1, or S2-IC1 antiserum cells. The NK cells appear by themselves when incubated with uncoated S2, as they did not adhere to the NK cells. Quantitative analyses of lytic granule distance from the MTOC are shown as a feature of the degree of granule convergence in YTS-CD16 (C) and eNK (D) cells. Data represent 30 cells per group, from three independent experiments for YTS-CD16 cells and three healthy donors for eNK cells. Gray points in each condition indicate the representative conjugates shown in A and B. Error bars show ± SD. **, $P < 0.01$; ***, $P < 0.001$; ****, $P < 0.0001$; ns, not significant.

these cells were conjugated with S2-IgG cells, degranulation events occurred outside the IS (Fig. 3 D, left), whereas with S2-IC1-IgG cells, degranulation was focused to the IS (Fig. 3 D, right). We additionally conjugated YTS-CD16-LAMP1-pHluorin cells to polystyrene beads coated with either anti-CD16 or anti-LFA-1 plus anti-CD16 and found that the former led to diffuse degranulation, whereas the latter led to degranulation focused to the bead (Fig. 3 E). Thus, NK cells activated by both CD16 and LFA-1 converged their granules and demonstrated highly focused synaptic degranulation, whereas those activated by CD16 did not, leading to nondirectional degranulation.

Directed secretion of lytic granules promotes specific killing of the targeted cell

To understand how directed versus nondirected degranulation might contribute to efficiency of NK cell cytotoxicity, we aspired to simulate tissue environments by creating aggregates of NK cells with various types of potential target cells that could be imaged by confocal microscopy to both track the movement of the lytic granules and quantify target cell death in real time. We used an UGATm system to create clusters of cells on demand, thus allowing us to exert control over the initiation of cell contact and signaling (Christakou et al., 2013). Viability of S2 cells and NK cells was not affected using the UGATm

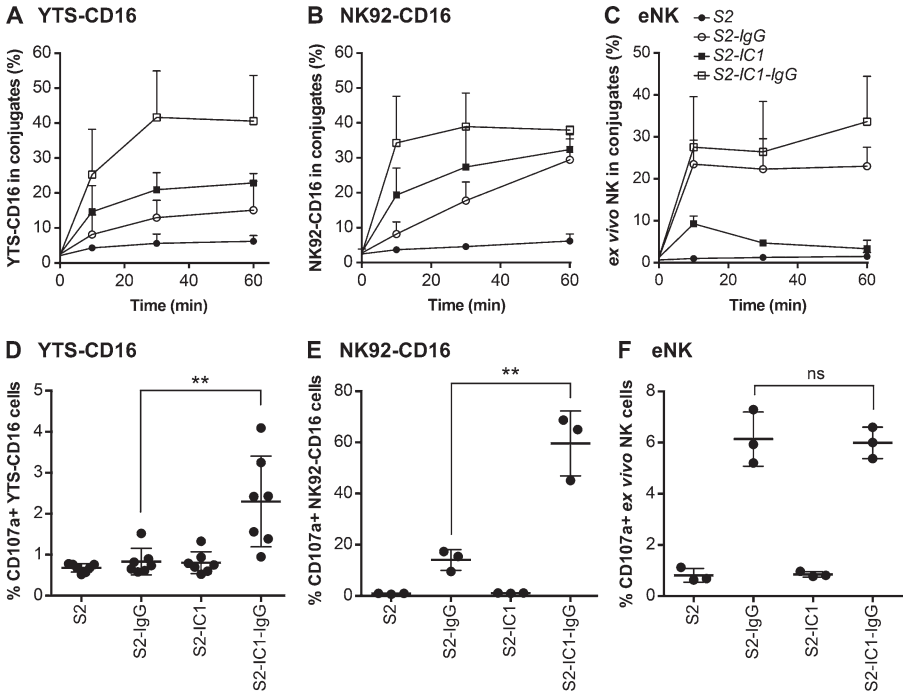

Figure 2. **CD16 engagement induces conjugate formation and degranulation in human NK cells.** For conjugation assay, numbers indicate the percentage of YTS-CD16 cells (A), NK92-CD16 cells (B), and previously cryopreserved eNK cells (C) in conjugates. Data represent results from three independent experiments using NK cell lines or eNK cells from three healthy donors. Error bars indicate + SD (A–C). For degranulation assay, combined results from seven experiments for for YTS-CD16 cells (D) and three experiments for NK92-CD16 cells (E) showed significantly higher degranulation levels of NK cells co-cultured with S2-IC1-IgG cells compared with S2-IgG cells. (F) Data from three healthy donors showed comparable degrees of degranulation by eNK cells coincubated with S2-IgG and S2-IC1-IgG cells. Error bars show ± SD (D–F). **, $P < 0.01$; ns, not significant.

system (unpublished data; Ohlin et al., 2015). NK cell lytic granules were tracked using LysoTracker red, and cell death was detected by uptake of SYTOX blue viability dye. Specific target cells were identified by preloaded vital dye. When YTS-CD16 cells were aggregated with S2-IgG cells, lytic granules remained diffusely distributed in the cytoplasm (Fig. 4 A and Video 1). When the same was performed with S2-IC1-IgG cells, the granules were highly converged and were polarized toward a target cell (Fig. 4 B and Video 2). The mean granule distance from the centroid was measured over time, showing that within 2-h intervals, lytic granules in YTS-CD16 cells aggregated with S2-IgG cells did not converge to the MTOC (Fig. 4 C). In contrast, those aggregated with S2-IC1-IgG cells had granules that were mostly converged by the time imaging could begin (consistent with our prior observations; Mentlik et al., 2010; James et al., 2013).

Killing efficiency was evaluated in these experiments and defined as the proportion of total target cells that assimilated viability dye. The killing efficiency over a given time frame was significantly higher in YTS-CD16 cells aggregated with S2-IC1-IgG cells compared with S2-IgG cells (Fig. 4 D). Over 2 h, YTS-CD16 cells aggregated with S2-IgG or S2-IC1-IgG cells induced a mean of ∼40% and ∼67% of killing, respectively. The same was true for eNK cells: when aggregated with S2-IgG cells, they demonstrated a significantly lower killing efficiency compared with that of S2-IC1-IgG cells: ∼25% and ∼59%, respectively (Fig. 4 E). This distinction in the eNK cells is important, because the total degranulation induced by the two different target cells was equivalent (Fig. 2 F). Thus directional degranulation triggered by the combined signals of CD16 and LFA-1 enhances the efficiency of target lysis by NK cells.

Nondirected degranulation increases bystander killing

In a physiological environment, NK cells are challenged with a need to discern diseased cells from those that are healthy (Eriksson et al., 1999). We hypothesize that NK cells use precise positioning of their cytolytic machinery to promote accurate target cell killing without collateral damage. To determine whether this precision was a feature of lytic granule convergence and directional degranulation, we performed the UGATm experiments with S2-IgG or S2-IC1-IgG cells but included differentially dye-labeled S2 cells. Thus yellow-labeled S2-IgG or S2-IC1-IgG target cells served as those capable of generating a signal for cytotoxicity, whereas green-labeled S2 cells served as "innocent bystanders." We measured granule positioning as well as death of the different target cells after aggregation with NK cells. As identified in experiments with only one type of target cell, YTS-CD16 cells aggregated with S2-IgG cells contained dispersed lytic granules (Fig. 5 A and Video 3), whereas those aggregated with S2-IC1-IgG cells had highly converged granules polarized toward the target cells (Fig. 5 B and Video 4). The lysis of S2 cells was calculated as a proportion of total target cell lysis to determine the degree of bystander killing by NK cells to account for the fact that the overall killing of S2-IgG cells was lower, likely as a feature of lesser signal input from this nonphysiological target cell system. The rate of bystander killing significantly increased by ∼17% when YTS-CD16 cells were aggregated with S2 and S2-IgG cells compared with S2 and S2-IC1-IgG (Fig. 5 C). To ensure the specificity of the target signal in these mixed-cell experiments, the transfer of anti–S2-IgG from S2-IgG cells to plain S2 cells in the cell mixture was measured and found to be negligible (Fig. S3, A and B). Thus, directed secretion provided higher specificity in target killing. This effect was even more striking when eNK cells were aggregated with S2-IgG or S2-IC1-IgG with S2 bystander cells. Nondirected secretion triggered by CD16 signaling alone caused 35% higher bystander killing than directed secretion activated by coengagement of CD16 and LFA-1 (Fig. 5 D). Thus, convergence of lytic granules, which promotes directed degranulation, therefore enables innocent bystander protection and allows for specificity of target killing.

To evaluate whether the lack of LFA-1 signaling reduced potential "sealing" of the IS and hence promoted bystander

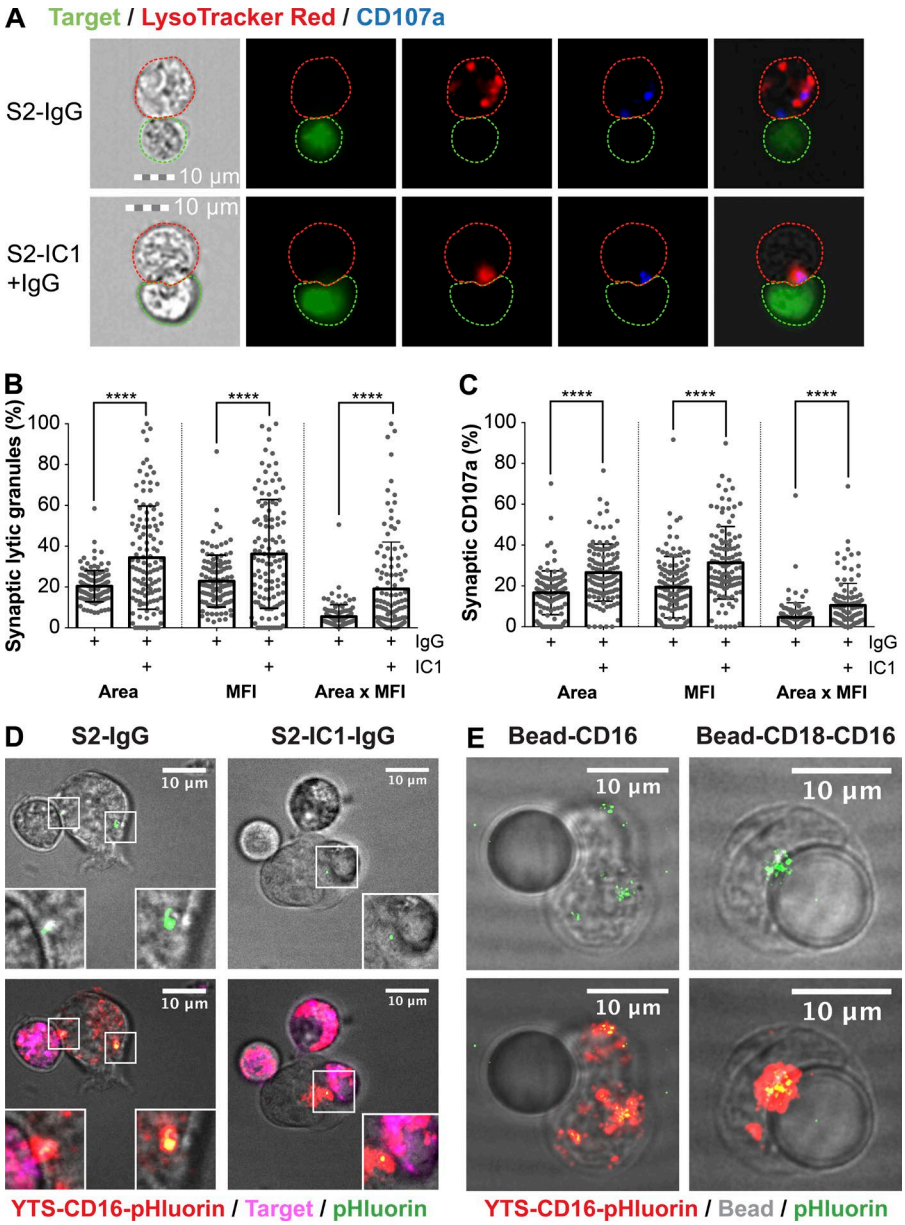

Figure 3. **Engagement of LFA-1 and CD16 induces more targeted degranulation at the IS than CD16 alone.** (A) Fixed-cell imaging flow cytometry of YTS-CD16 cells conjugated with S2-IgG or S2-IC1-IgG cells. Quantitative analyses of area, mean fluorescence intensity (MFI), and total fluorescence intensity (area × MFI) of LysoTracker red (lytic granules; B) and CD107a (C) staining at the immunological synapse are shown as a feature of directed degranulation of YTS-CD16 cells. Data represent pooled results from three independent experiments; $n > 100$ cells/group. Error bars show ± SD. Live-cell confocal microscopy of YTS-CD16 cells transduced with a degranulation indicator LAMP1-pHluorin construct conjugated with S2-IgG or S2-IC1-IgG cells (D) or 10 µm polystyrene beads coated with anti-CD16 or anti-CD18 plus anti-CD16 antibody (E). Magenta, target cells; red, LysoTracker red (lytic granules); green, pHluorin (degranulation events). ****, $P < 0.0001$.

killing by polarized degranulation events, the geometry of the synapse formed between YTS-CD16 cells and S2-IgG or S2-IC1-IgG cells was measured (Fig. 6 A). Although fewer lytic granules were at the synapse with the S2-IgG cells (Fig. 6 B, consistent with Fig. 3 B), the length of the synapse was not different from that formed with S2-IC1-IgG cells (Fig. 6 C). Furthermore, the length of the IS as a feature of the perimeter of both the effector (Fig. 6 D) and target (Fig. 6 E) cell was also not different between the S2-IgG and S2-IC1-IgG cells. This suggests that the contact is not partial in S2-IgG and that it is indeed the nondirected release of granules away from the target that promotes bystander destruction.

In our previous studies, we showed that granule convergence is dynein dependent (Mentlik et al., 2010). To further test our hypothesis regarding the role for convergence in promoting killing efficiency and protecting bystanders, we used a small-molecule dynein inhibitor, ciliobrevin D (Firestone et al., 2012), to block the convergence of lytic granules to the MTOC from their dispersed localization in the cytoplasm. This allowed us to manipulate granule trafficking via blocking the motor protein function, instead of altering activating signal input. YTS, NK92, or eNK cells were treated with either ciliobrevin D or vehicle and conjugated with their respective target cells. Compared with vehicle control, ciliobrevin D treatment blocked lytic granule convergence in YTS (Fig. 7, A and D), NK92 (Fig. 7, B and E), and eNK (Fig. 7, C and F) cells as determined by mean granule-to-MTOC distance. As a separate measure of granule dispersion, the standard deviation of the granule-to-MTOC distance was calculated to show the degree of scatter of individual lytic granules. This was also increased by ciliobrevin D in YTS (Fig. 7 G), NK92 (Fig. 7 H), and eNK (Fig. 7 I) cells. CD107a staining was additionally performed to test whether ciliobrevin D treatment affected the exocytosis of lytic granules; the proportion of eNK cells that degranulated after treatment with ciliobrevin D increased slightly (Fig. S4 A), whereas in the NK cell lines it decreased (Fig. S4, B and C). In all cases, however, degranulation still occurred in the presence of ciliobrevin D.

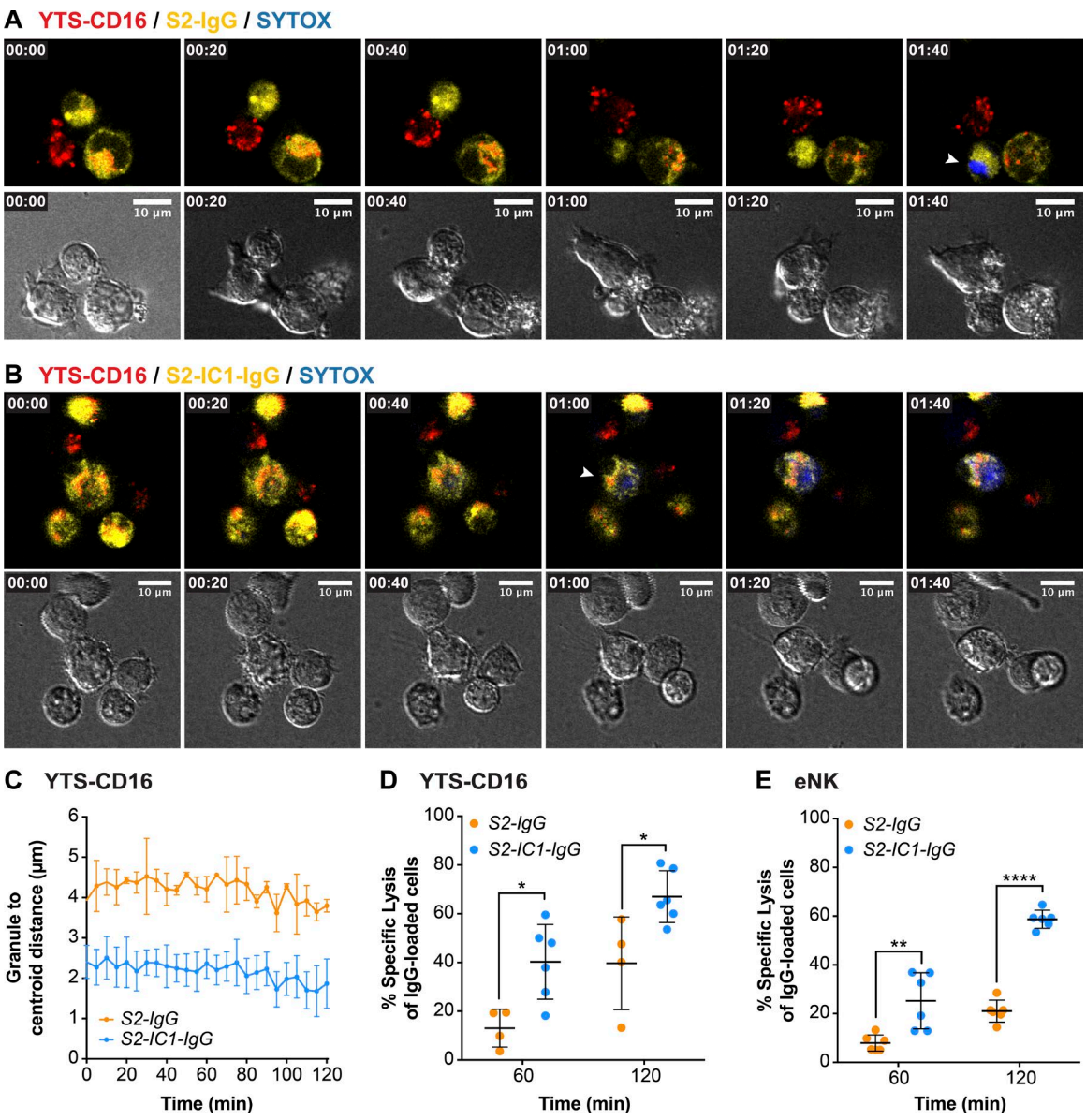

Figure 4. **Targeted secretion of lytic granules promotes more killing of the target cells.** Live-cell confocal microscopy of YTS-CD16 cells conjugated with S2-IgG (A) or S2-IC1-IgG (B) cells. NK cells were mixed with the target cells immediately before the imaging process. Cell mixtures were imaged every 5 min for 2 h. Time zero represents the start of imaging. Yellow, S2-IgG or S2-IC1-IgG cells; red, LysoTracker red (lytic granules); blue, SYTOX blue viability dye. Quantitative analyses of viable cells are shown as a feature of the differential killing efficiency. Arrowheads indicate uptake of SYTOX blue viability dye by the target cells. (C) Live granule tracking in YTS-CD16 cells conjugated with S2-IgG and S2-IC1-IgG cells, respectively. Each point indicates one independent experiment using YTS-CD16 (D) and eNK (E) cells ($n > 300$ cells/group). Error bars show ± SD. *, $P < 0.05$; **, $P < 0.01$; ****, $P < 0.0001$.

Because directed degranulation with converged granules promoted killing efficiency, we wanted to use ciliobrevin D to physically prevent convergence in a cell that had received a convergence signal. We hypothesized that this would allow us to abrogate the killing efficiency benefit imparted by lytic granule convergence. To measure killing of both the target and bystander cells in a single experiment, we performed flow cytometry–based cytotoxicity assays, wherein each cell line was labeled with a unique fluorescent dye in the presence of medium containing SYTOX blue viability indicator dye. NK cell–resistant Raji B lymphoblastoid cells were used as bystanders, susceptible 721.221 or K562 cells were used as inciting target cells, and both were incubated with YTS, NK92, or eNK cells that had been treated with DMSO or ciliobrevin D. In the absence of Raji bystander cells, ciliobrevin D did not affect killing of 721.221 or K562 cells (Fig. S5, A–C). When Raji cells were added, ciliobrevin D–treated YTS (Fig. 8 A), NK92 (Fig. 8 B), and eNK (Fig. 8 C) cells again showed no change in killing of 721.221 or K562 cells (Fig. 8, A–C, left) but now demonstrated killing of the bystander Raji cells in a dose-dependent manner (Fig. 8, A–C, right). The viability of YTS (Fig. S5, D and G), NK92 (Fig. S5, E and H), and eNK (Fig. S5, F and I) cells was not affected by DMSO or ciliobrevin D treatments. Using standard ^{51}Cr-release assays, we additionally analyzed the lysis of susceptible 721.221 and K562 cells by YTS (Fig. S4 D) and NK92 (Fig. S4 E) cells, respectively, with and without ciliobrevin D and found that ciliobrevin D did not substantively alter total killing. To ask whether it promoted more collateral

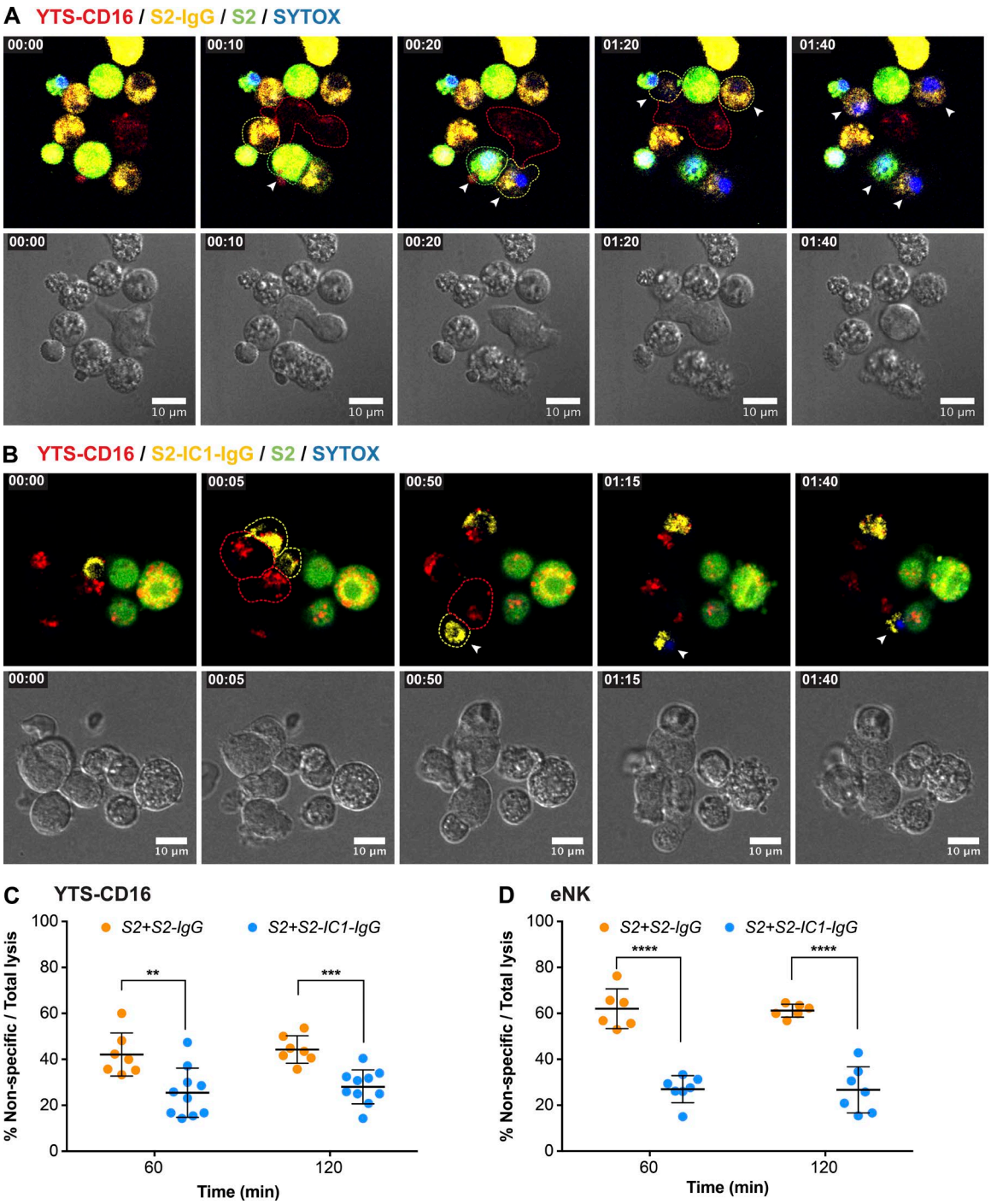

Figure 5. **Nondirected degranulation outside of the IS increases bystander killing of the neighboring cells.** Live-cell confocal microscopy of YTS-CD16 cells incubated with S2 cells as innocent bystanders and S2-IgG (A) or S2-IC1-IgG (B) cells as activating targets. NK cells were mixed with the target cells immediately before the imaging process and imaged every 5 min for 2 h. Yellow, IgG-labeled S2 or S2-IC1 cells; green, bystander S2 cells; red, LysoTracker red (lytic granules); blue, SYTOX blue viability dye. Arrowheads indicate uptake of SYTOX blue viability dye by the target/bystander cells. Quantitative analyses of nonspecific killing of S2 cells over total lysis are shown as a feature of collateral damage to the bystander S2 cells by YTS-CD16 (C) and eNK (D) cells. Each point indicates one independent experiment; $n > 400$ cells/group. Error bars show ± SD. **, $P < 0.01$; ***, $P < 0.001$; ****, $P < 0.0001$.

damage by NK cells, we added ^{51}Cr-labeled Raji cells (to serve as innocent bystanders) along with unlabeled 721.221 or K562 target cells. Compared with DMSO-treated control YTS (Fig. S4 D) and NK92 (Fig. S4 E) cells, those treated with ciliobrevin D caused more nonspecific lysis of the Raji cells. YTS or NK92 cells co-cultured with ^{51}Cr-labeled Raji cells in the absence of 721.221 or K562 were unable to kill Raji cells (Fig. S5 J). Thus ciliobrevin D treatment prevented lytic granule convergence and promoted greater collateral damage even when a convergence signal was present. Convergence therefore serves to protect innocent bystander cells in complex cellular environments.

To apply this concept in the context of physiological antibody-dependent cell-mediated cytotoxicity (ADCC), we used a human therapeutic monoclonal antibody, rituximab (RTX),

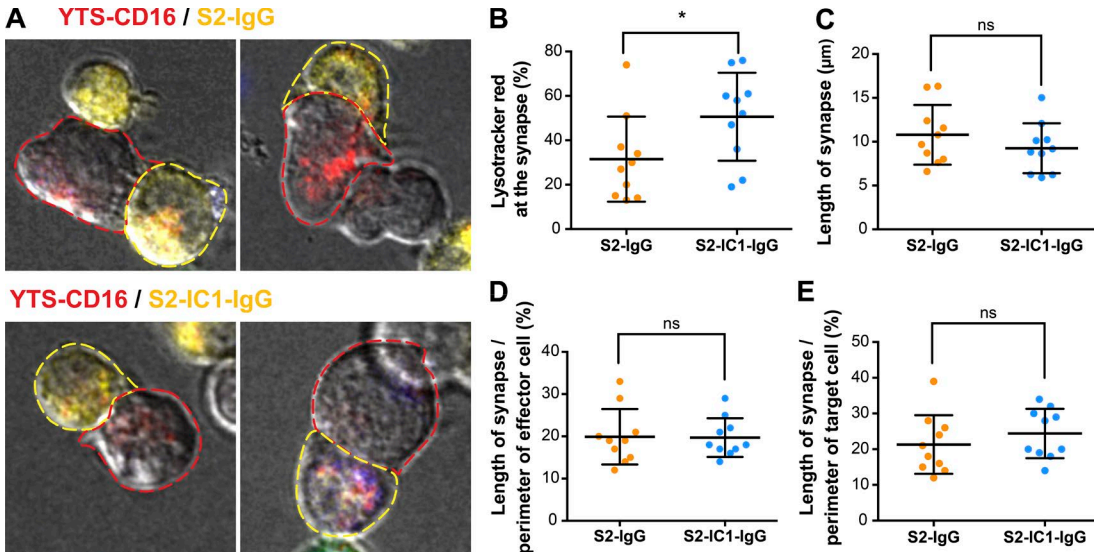

Figure 6. **CD16 ligation alone induces IS geometry similar to that of the IS engaging both LFA-1 and CD16.** (A) Example confocal microscopy images of YTS-CD16 cells mixed with differentially labeled S2 cells as performed in Fig. 5. Cell outlines are drawn to indicate the perimeter of the conjugate analyzed (yellow, target; red, effector). Quantitative analyses of the total fluorescence intensity of LysoTracker red at the synapse (B), the length of synapse (C), and the percentage of the perimeter of the cell involved engaged in the synapse from the standpoint of the effector (D) or the target (E). Error bars show ± SD. *, $P < 0.05$; ns, not significant.

along with NK cell–resistant Raji cells that naturally express the antigen recognized by RTX. Here we used UGATm to aggregate eNK cells with yellow dye–labeled uncoated Raji cells and green dye–labeled RTX-coated Raji cells, all in the presence of SYTOX blue viability dye. In this setting, there was preferential killing of the RTX-coated Raji cells (Fig. 9, A and C; and Video 5). When LFA-1 engagement was prevented, however, by treating eNK cells with LFA-1-blocking antibody, there was significantly increased killing of uncoated Raji cells (Fig. 9, B and C; and Video 6). The same result was found on a population basis when the same cell combinations were used in a ^{51}Cr-release assay: the addition of LFA-1 blockade led to greater destruction of the otherwise resistant Raji cells (Fig. 9 D). Thus the engagement of LFA-1 by the inciting target cell prevents bystander killing. This, in concert with our ciliobrevin D findings, uncovers a potentially useful strategy to control cytotoxic cells to promote collateral damage.

Discussion

NK cell activation triggers stepwise cellular events, leading to secretion of lytic granules and lysis of diseased cells. A characteristic step in this process of unknown significance is that of lytic granule convergence to the MTOC after NK cell activation. As shown previously, lytic granule convergence precedes MTOC/granule polarization, is independent of actin rearrangement/microtubule dynamics and calcium mobilization, and depends on specific signaling requirements downstream of β2 integrin (Mentlik et al., 2010; James et al., 2013; Zhang et al., 2014). Although the process of convergence itself is established, its contribution to cytotoxicity has not been. In our aim to elucidate how lytic granule convergence might contribute to NK cell cytotoxicity, one of our major challenges was to specifically access and block granule convergence without impairing the downstream cytolytic functions. To overcome this difficulty, we used a surrogate experimental target cell system of *Drosophila* S2 cells. Advancing prior work in the signaling for convergence (James et al., 2013; Zhang et al., 2014), we provided NK cells with specific combinations of signal inputs to precisely experimentally control granule convergence and degranulation: LFA-1 ligation triggers lytic granule convergence but not degranulation, whereas CD16 ligation induces degranulation without convergence. We used this dichotomy to functionally dissect any contribution of convergence to cytotoxicity.

Through the use of an UGATm system, we were able to precisely govern and image the beginning of contact between NK and target cells to fully appreciate the positioning of lytic granules after reception of the activation signaling (while monitoring the viability of all cells). This approach allowed us to move beyond chance events and methodically collect replicates for quantitative analysis of granule dynamics. After combining NK cells expressing our previously reported degranulation indicator (Rak et al., 2011), we were able to coordinate granule positioning with the directionality of secretion. We also were able to complement these approaches with imaging flow cytometry for the purpose of mass data collection, with spatial localization providing the additional advantage of not having to adhere cells to glass surfaces. Combining these approaches, we demonstrated that granule convergence induced by LFA-1 engagement leads to more targeted secretion at the IS. In comparison, granules remaining dispersed in NK cells conjugated with S2 IgG cells degranulated not only at the IS but also at other locations (a result confirmed using anti-receptor antibody–coated polystyrene beads and LAMP1-pHluorin cells). This dichotomy allowed us to ask how directional versus nondirectional degranulation impacts the cytolytic activity of NK cells. We hypothesized that convergence served as a preparatory step to help promote targeted killing of transformed target cells while preserving the healthy surrounding tissue.

Without converged granules, NK cell killing efficiency was drastically reduced when measured by specific lysis of inciting target cells over time. Because eNK cells conjugated with S2-IgG or S2-IC1-IgG cells resulted in comparable

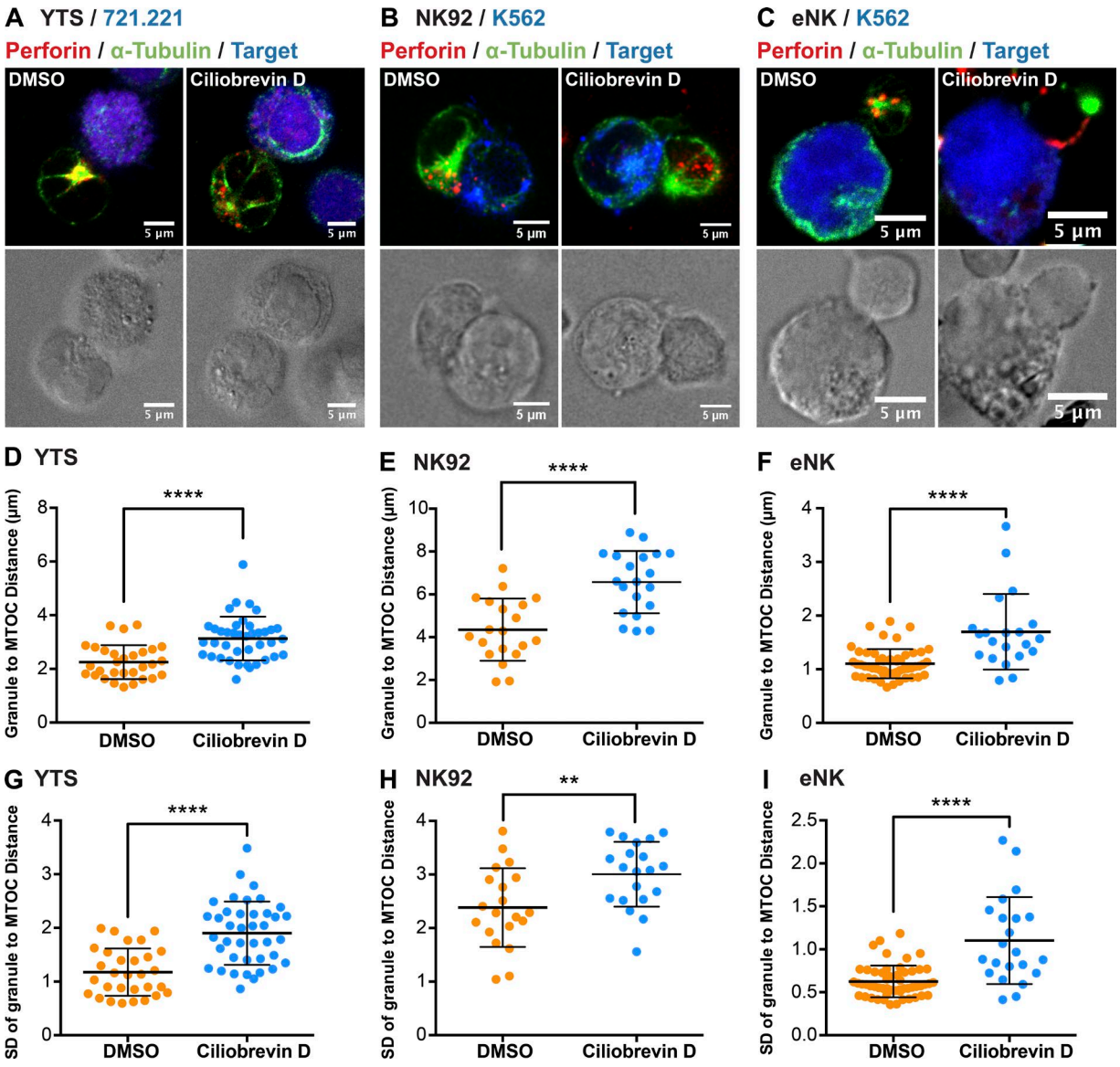

Figure 7. **Ciliobrevin D inhibits granule convergence in NK cells.** Fixed-cell confocal microscopy of YTS (A), NK92 (B), and eNK (C) cells conjugated with their respective target cells after DMSO or ciliobrevin D treatment (100 µM). Red, anti-perforin; blue, 721.221 or K562 cells; green, anti–α-tubulin. Quantitative analyses of the mean lytic granule distance from the MTOC and its SD are shown as a feature of the degree of granule convergence in YTS (D and G), NK92 (E and H), and eNK (F and I) cells. Data represent pooled results from two independent experiments for YTS cells and NK92 cells and two healthy donors for eNK cells (n > 20 cells/group). Error bars show ± SD. **, P < 0.01; ****, P < 0.0001.

degranulation levels and similar IS geometries, the lack of converging granules is likely to be the major cause of the reduced killing efficiency in our study. Therefore, lytic granule convergence serves as a prerequisite step enabling NK cells to compress their cytolytic cargo and allow for focused release of their lytic contents to promote efficient target cell lysis. Thus, when considering how an NK cell may navigate a complex tissue comprised mostly of healthy cells to "seek and destroy" diseased cells, their convergence strategy emerges as fundamental.

As an important demonstration, in our experiments CD16 signaling alone caused significantly higher nonspecific killing of bystander target cells compared with the combined signals of CD16 and LFA-1. As we have previously shown, NK cells from leukocyte adhesion deficiency-1 patients, who lack LFA-1, could not converge lytic granules and had inefficient cytolytic activity (James et al., 2013). Because ICAM-1 is expressed on a variety of mammalian cell types (Hubbard and Rothlein, 2000; Ramos et al., 2014), it likely serves as a near-omnipresent facilitator to promote NK cell–targeted attacks within healthy tissues, as simulated using our UGATm-induced cell aggregates. Therefore, LFA-1 promoting lytic granule convergence may be evolutionarily preserved as the prerequisite mechanism to ensure the specificity of NK cell cytotoxicity. This concept is underscored further by our results using LFA-1 blockade, as doing so in the presence of an inciting IgG-coated physiological target cell causes the increased death of noninciting surrounding cells.

It is relevant to note that although CD16 signaling alone from an opsonized target cell does not lead to granule convergence in NK cells, the combination of CD16 and LFA-1 in our experiments further reduced the mean distance of lytic granules to the MTOC compared with LFA-1 alone. This suggests that CD16 signaling in concert with the true convergence signal can

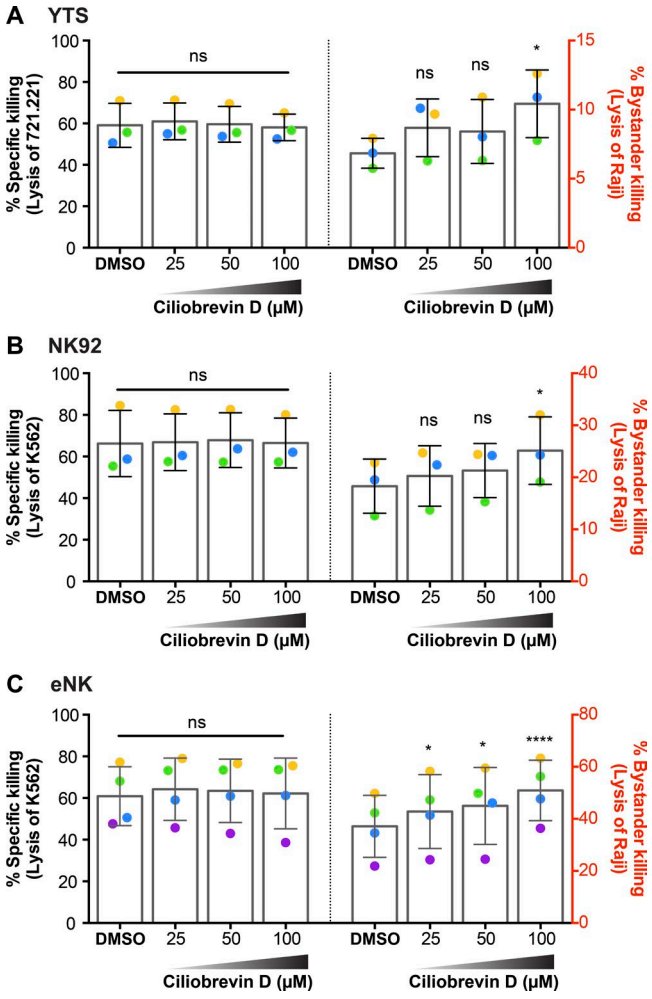

Figure 8. **Ciliobrevin D increases bystander killing of the neighboring cells.** Flow cytometry–based cytotoxicity assay of NK cells treated with ciliobrevin D or DMSO control was performed as described in Materials and methods. Raji cells were used as nonsusceptible bystander cells to measure the degree of collateral damage caused by nondirectional degranulation. Specific lysis of the corresponding susceptible targets 721.221 and K562 cells by YTS (A, left) and NK92 (B, left) cells was not affected by ciliobrevin D treatment, whereas the nonspecific lysis of Raji cells by YTS (A, right) and NK92 (B, right) cells increased after ciliobrevin D treatment (100 µM) compared with DMSO control. The cytotoxic function of eNK cells against K562 cells was also not affected (C, left), and the bystander killing of Raji cells was increased (C, right). Data from three independent experiments for YTS and NK92 cells and three healthy donors for eNK cells is shown. Colored dots denote individual experiments or donors. Error bars show ± SD. *, $P < 0.05$; ****, $P < 0.0001$; ns, not significant.

also add to lytic granule convergence. This may also in part explain why very high concentrations of anti-S2 rabbit antiserum had been previously observed to induce low levels of lytic granule convergence in eNK cells (Zhang et al., 2014). This may have additionally been a feature of that study having used diluted rabbit serum, as we did not identify this effect in our experiments using purified anti–S2-IgG. Regardless, the concepts do speak to the important overlap in and interplay between LFA-1 and CD16 signaling pathways, even though that of CD16 is missing key elements to efficiently initiate convergence (Zhang et al., 2014). In this light, the upstream signaling components common to both pathways remains to be fully established.

The preformed lytic granules in NK cells are lysosome-related organelles that comprise a cell type–specific subcellular compartment, which, as the secretory lysosomes in hematopoietic cells, are comparable to the Weibel-Palade bodies (WPBs) in endothelial cells (Marks et al., 2013). Secretory lysosomes are dual-function organelles that share features with both conventional secretory and endocytic pathways (Blott and Griffiths, 2002). Examples include lytic granules in NK cells and CTLs, dense granules in platelets, histamine-containing granules in mast cells and basophils, and melanosomes in melanocytes. Secretory lysosomes share certain molecular requirements for secretion. For example, Rab27a facilitates tethering of lytic granules (Elstak et al., 2011; Kurowska et al., 2012), melanosomes (Hume and Seabra, 2011), and WPBs (Zografou et al., 2012); partially overlapping vSNARE and Munc complexes promote docking of lytic granules (Feldmann et al., 2003) and dense granules (Ren et al., 2010). As a distinct characteristic of NK cells and CTLs, however, lytic granules traffic to the MTOC using dynein (Mentlik et al., 2010; Ritter et al., 2015) before polarizing toward the cell periphery, allowing for the tethering and docking processes. Melanocytes, for example, also transport melanosomes in a minus end–directed manner using dynein function, but that only serves to aggregate melanosomes at the MTOC, which prevents secretion of pigments (Nilsson et al., 1996; Nascimento et al., 2003) and as such is more typical of secretory lysosome regulation across cell types. Of note, NK cells do converge lytic granules in noncytolytic conjugates (Mentlik et al., 2010), possibly leading to this same outcome, to prevent undesired granule secretion onto innocent targets. Thus, when an NK cell enters a cellular tissue environment and is exposed to adhesion via an integrin signal, it likely first converges its granules to protect the tissue itself and provide the opportunity to further sense and integrate signals for targeted killing of the diseased cells within a mostly healthy tissue.

In light of the mechanism driving convergence, we hypothesized that through specifically inhibiting dynein in NK cells that have received a convergence activation signal, this protective mechanism can be bypassed, forcing lytic granules to degranulate nondirectionally, leading to increased nondiscriminant bystander killing. As a proof of concept, we used ciliobrevin D, a small-molecule inhibitor of cytoplasmic dynein, to block granule convergence in NK cells. Indeed, ciliobrevin D treatment led to a dose-dependent increase of collateral killing against the nonsusceptible bystander cells while maintaining the killing rate of the sensitive target cells. This approach allowed us to demonstrate how an inability to converge lytic granules in activated NK cells may nonspecifically kill neighboring innocent cells in a more physiologically relevant setting. Along these lines, we also approached the same concept using the blockade of LFA-1 to prevent convergence, but here with the clinically relevant IgG molecule RTX to provide the degranulation signal. As was the case with ciliobrevin D treatment, blocking convergence by blocking LFA-1 promoted the killing of otherwise nonsusceptible bystander cells.

Importantly, these observations provide potential therapeutic insight, as nondirectional degranulation may be useful in the setting of cellular therapies using cytotoxic cells or therapeutic monoclonal antibodies (such as RTX). Cytotoxic cells infused into patients for anticancer therapy (also referred to as cell therapy) has led to major advances and provided great hope in clinical medicine (Fesnak et al., 2016; Jackson et al., 2016). Cell therapy cells are highly activated and express integrin as well as exogenously introduced activation receptors to allow them to destroy cancer cells after specific recognition

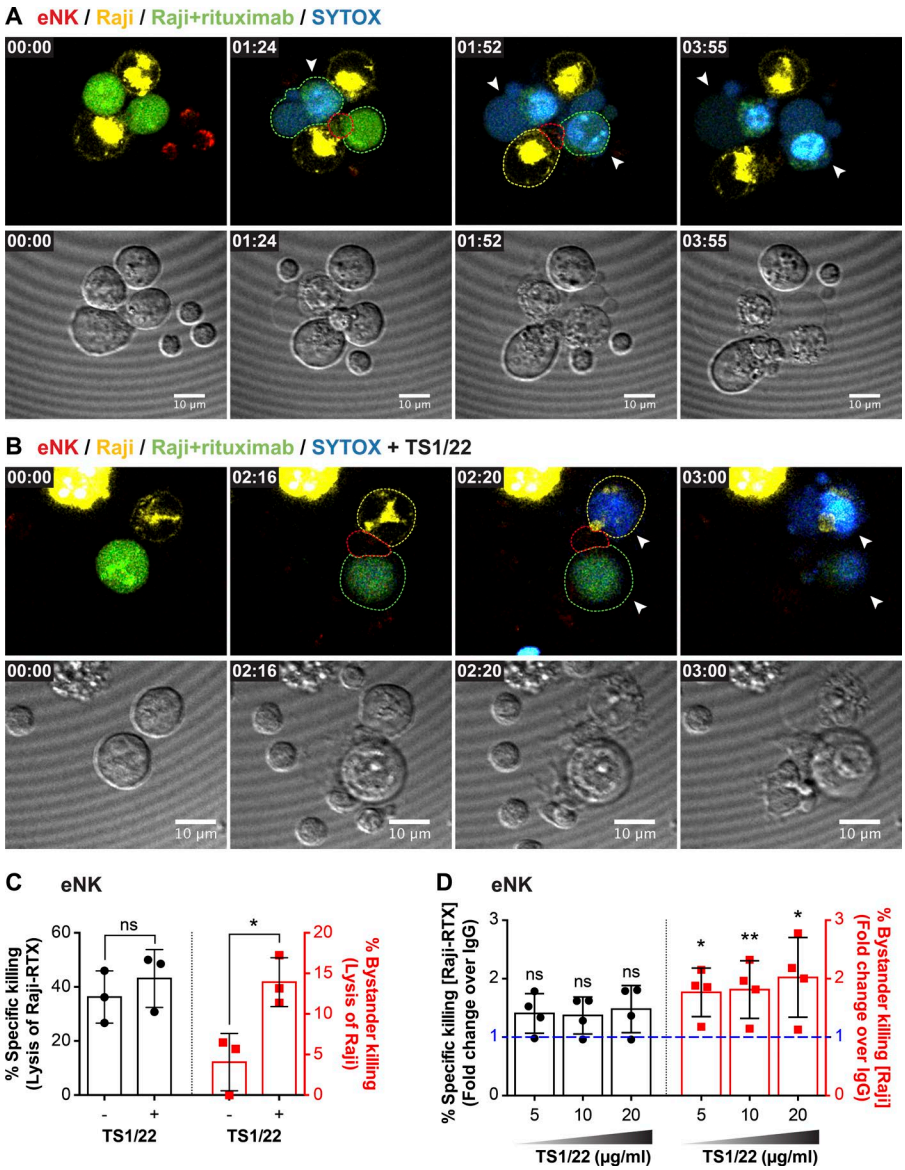

Figure 9. **LFA-1 blockade increases bystander killing.** Live-cell confocal microscopy of antibody-dependent cellular cytotoxicity by eNK cells treated with murine IgG1 mAb control (A) or LFA-1 blocking mAb (clone TS1/22; B). Green, RTX-coated Raji cells (NK-inciting targets); yellow, uncoated Raji cells (bystanders); red, LysoTracker red (lytic granules); blue, SYTOX blue viability dye. NK cells were mixed with the target cells immediately before the imaging process and imaged every 4 min for 4 h. Quantitative analyses of viable cells are shown to demonstrate specific (C, left) versus nonspecific (C, right) killing by eNK cells. Data represent combined results from three healthy donors. Standard 4 h ^{51}Cr cytotoxicity assay of NK cells treated with LFA-1–blocking mAb or murine IgG control (D). Each dot represents an individual healthy donor. Error bars show ± SD. *, $P < 0.05$; **, $P < 0.01$; ns, not significant.

of a cancer-specific ligand. Initial cellular studies have demonstrated converged and polarized lytic granules in therapy cells conjugated with tumor cell targets (Hegde et al., 2016). Although cytotoxic cells excel in eliminating individual diseased cells, an established tumor contains many diseased cells, some of which are in the process of immune escape. Thus converged and polarized lytic granules in therapy cells may not be the most effective in the eradication of a massive tumor by those therapy cells that have trafficked into the tumor environment. In this instance, preventing lytic granule convergence in therapy cells (perhaps by pretreating them with ciliobrevin D itself or anti–LFA-1) before their infusion into a patient may allow for broad-scale diffuse degranulation, with "collateral damage" mediated by transferred cells that have received a degranulation signal. This could allow therapy cells that have entered a tumor to promote more widespread killing, potentially providing greater tumor cell killing per therapy cell as well as promoting killing of tumor cells in the process of immune escape. This is likely a different task from that NK cells have evolved to excel at, which is precision seek-and-destroy missions protecting healthy surrounding tissues and the killing of single diseased cells before they establish a tumor. The same approach could be envisioned as an adjunct therapy for patients receiving a monoclonal antibody to treat cancer, although this would require an additional treatment to patients because the therapeutic antibodies use a patient's endogenous cytotoxic cells. Thus, although these immune-based therapies may be effective, there may be substantive room for improvement by exploiting the cell biology of cytotoxicity and lytic granule positioning.

Collectively, these results have shown for the first time that NK cells can cause collateral damage to healthy bystander cells using nondirected degranulation. That is, lytic granule convergence plays an essential role in regulating the pointed and focused secretion of the cytolytic granule contents. As such, lytic granule convergence in NK cells and CTLs may serve as the primary regulatory step for promoting precision of targeted killing and diminishing occurrence of bystander killing. The nondirectional degranulation pathway induced by CD16 signaling, however, is likely to also exist for evolutionarily relevant reasons. For one, it may serve as a natural "last chance" effort against growing tumors, as ICAM-1 expression is often down-regulated in established tumor cells, which renders them resistant to CTL

lysis (Blank et al., 2005; Hamaï et al., 2008), but may allow for an NK cell–perceived danger signal to provide diffuse degranulation in the tumor cell environment (Stojanovic and Cerwenka, 2011; Gras Navarro et al., 2015). More importantly, however, nondirected secretion may function in the elimination of opsonized nonhuman pathogens in a pathogen-rich environment (Jones et al., 2009; Lu et al., 2014), allowing an entering NK cell to destroy large numbers of organisms, only a few of which may be coated with host-produced IgG (directly analogous to the S2-IgG cells). Thus, by understanding the role convergence plays in NK cell cytotoxicity, we expect that a powerful regulatory step in NK cell cytotoxicity can be harnessed and exploited for tailoring and improving immunological therapies.

Materials and methods

Cell lines and eNK cells

The immortalized human NK cell lines YTS and NK92 were maintained as described previously (James et al., 2013). The YTS-CD16 cell line was a gift from J. Coligan and K. Krzewski (National Institutes of Health, Bethesda, MD; Peruzzi et al., 2013). The NK92-CD16 cell line was a gift from K. Campbell (Fox Chase Cancer Center, Philadelphia, PA; Binyamin et al., 2008). Human eNK cells were prepared from peripheral blood of healthy donors by standard Ficoll-Paque isolation followed by negative selection (Miltenyi Biotec). All human blood samples were obtained in accordance with the Institutional Review Board for the Protection of Human Subjects of Baylor College of Medicine. The *Drosophila* S2 and S2-ICAM-1 (S2-IC1) Schneider cell lines were provided by D. Liu (Houston Methodist Hospital, Houston, TX) and were used as surrogate targets for YTS-CD16, NK92-CD16, and eNK cells, which were maintained as previously described (James et al., 2013). The 721.221 cell line was used as susceptible target cells for YTS and YTS-CD16 cells and the K562 cell line as target cells for NK92, NK92-CD16, and eNK cells. The Raji cell line was used as nonsusceptible target cells in the bystander cytotoxicity assay for YTS, NK92, and eNK cells. YTS-CD16 cells were transduced to stably express LAMP-1-pHluorin as described previously (Rak et al., 2011).

Live-cell confocal microscopy

YTS-CD16 and eNK cells were incubated with 5 µM LysoTracker red DND-99 (Thermo Fisher Scientific) for 30 min at 37°C and washed. S2 and S2-IC1 cells were preincubated with anti-S2 polyclonal IgG for 30 min, washed, and labeled with cell proliferation dye eFluor670 (eBioscience). For bystander killing assays, S2 cells were labeled with CellTrace CFSE cell proliferation dye (Thermo Fisher Scientific) to differentiate them from the S2-IgG or S2-IC1-IgG cells. NK and target cells were mixed at a ratio of 1:3 to a final volume of 200 µl in complete R10 medium supplemented with 5 µM SYTOX blue viability dye (Thermo Fisher Scientific). Cell mixtures were then added directly onto the chip of the UGATm device to allow clustering of cells in the central area of each microwell (Christakou et al., 2013). Cells in the microwells were imaged using a Leica Microsystems SP8 laser scanning confocal microscope with a 100× magnification, 1.4-NA objective. Excitation was provided by a UV laser at 405 nm and tunable white light laser at 488, 561, and 647 nm. Emission was detected with HyD detectors, and images were collected in a single *z*-plane at one frame every 4 or 30 min for 120 min. Data were acquired with LAS AF software (Leica Microsystems) and subsequently exported to Volocity software (PerkinElmer) for further analysis. For imaging of ADCC, eNK cells, Raji cells, and RTX-coated Raji cells were labeled with LysoTracker red DND-99, cell proliferation dye eFluor670, and CellTracker green (all fromThermo Fisher Scientific), respectively. Cells were then mixed at a 1:3:3 ratio in 200 µl R10 medium supplemented with SYTOX blue viability dye in the presence of control murine IgG1 mAb or anti-CD11a blocking mAb. Images were taken every 4 min for 4 h. For live degranulation imaging, YTS-CD16-LAMP1-pHluorin cells were loaded with LysoTracker red and incubated with S2-IgG or S2-IC1-IgG cells labeled with eFluor670 proliferation dye or antibody-coated polystyrene beads. 10-µm polystyrene beads (Polysciences) were coated with 10 µg of anti-CD16 mAb (clone 3G8) or anti-CD16 and anti-CD8 (clone IB4) mAb for 30 min at 37°C, washed once with PBS, and added to the YTS-CD16-LAMP1-pHluorin cells. Cell mixtures were then immediately applied onto the microwells for imaging as described previously (Rak et al., 2011).

Fixed-cell confocal microscopy

YTS-CD16, NK92-CD16, or eNK cells co-cultured with S2, S2-IgG, S2-IC1, or S2-IC1-IgG cells for 15 min were adhered to poly-L-lysine–coated glass slides for 20 min at 37°C. The surrogate target S2 cells were previously labeled with CellTracker orange (Thermo Fisher Scientific). Fixation, permeabilization, and staining were performed as described (Banerjee et al., 2007). The reagents/antibodies were used in the following sequence for optimized results: (1) biotinylated monoclonal mouse anti-tubulin (Invitrogen); (2) streptavidin–Pacific blue (Invitrogen); and (3) FITC-conjugated mouse anti-perforin clone δG9 (BD). Slides were mounted with 0.15-mm coverslips (VWR) using ProLong AntiFade (Invitrogen). The image acquisition settings were as described in "Live-cell confocal microscopy," and all transmitted light images were specifically from the focal plane of the MTOC of the NK cell, which may not have been ideal for those images, especially the conjugated target cell, and are thus provided for orientation only.

Flow cytometry–based conjugation assay

YTS-CD16, NK92-CD16, and eNK cells were labeled with CellTrace CFSE for 10 min at RT. S2 and S2-IC1 cells were preincubated with S2 antiserum or anti-S2 polyclonal IgG antibody at a final dilution of 1:1,000 for 30 min at RT and washed three times. S2, S2-IgG, S2-IC1, and S2-IC1-IgG cells were then labeled with cell proliferation dye eFluor 670 for 5 min at RT. 10^5 NK cells and 2×10^5 target cells were mixed in 200 µl complete R10, incubated for the indicated times at 37°C (0, 10, 30, or 60 min), vortexed, and fixed with 1% PFA in PBS. Cell mixtures were run on an LSRFortessa flow cytometer (BD), and data were analyzed using FlowJo X (Tree Star).

Flow cytometry–based degranulation assay

YTS-CD16, NK92-CD16, and eNK cells were labeled with CellTrace CFSE for 10 min at RT. S2 and S2-IC1 cells were preincubated with anti-S2 polyclonal IgG antibody at a final dilution of 1:1,000 for 30 min at RT and washed three times. S2, S2-IgG, S2-IC1, and S2-IC1-IgG cells were then labeled with cell proliferation dye eFluor 670 for 5 min at RT. 10^5 NK cells and 2×10^5 target cells were mixed in 200 µl complete R10, incubated for 2 h at 37°C in the presence of anti-CD107a antibody and GolgiStop (BD), fixed with 1% PFA in PBS, and analyzed as described in "Flow cytometry–based conjugation assay."

Flow cytometry–based cytotoxicity assay

YTS-CD16, NK92-CD16, and eNK cells were labeled with CellTrace CFSE for 10 min at RT, washed, and treated with ciliobrevin D or DMSO control as described in the Inhibitors section. 721.221 and K562 cells were labeled with cell proliferation dye eFluor 670 for 5 min at RT. Raji cells were labeled with PKH-26 according to the manufacturer's protocol (Sigma-Aldrich). NK cells were then mixed with the corresponding targets and Raji cells at a final volume of 200 µl

in complete R10 and incubated at 37°C for 2 h. Cells were then labeled with SYTOX blue viability dye for 5 min at RT, washed, and run on LSRFortessa flow cytometer (BD).

^{51}Cr-release assay

Target cells (721.221 or K562) were incubated with 100 µCi ^{51}Cr (Na_2CrO_4; PerkinElmer) per 10^6 cells at 37°C for 1 h, washed four times, and resuspended in complete R10 medium at a concentration of 10^5 cells/ml. 10^4 ^{51}Cr-labeled cells were dispensed into each well of a 96-well, round-bottomed polystyrene plate, mixed with NK cells at specified effector/target ratios, and incubated at 37°C for 4 h. 100 µl of the supernatants was transferred from each well into corresponding wells in a LumaPlate-96 (PerkinElmer) and allowed to dry overnight. ^{51}Cr released into supernatants was measured using a TopCount NXT (PerkinElmer). Percentage lysis was calculated as follows: 100 × [(expected cpm − spontaneously released cpm)/(total cpm − spontaneously released cpm)]. Total cpm was assessed by complete lysis of target cells using 1% IGEPAL (Sigma-Aldrich) in water (Orange et al., 2011). Where indicated, ^{51}Cr-labeled bystander cells (Raji cells) were mixed with unlabeled target cells (721.221, K562, or RTX-Raji cells) to test the indirect lysis of unlabeled bystander targets. For ADCC, Raji cells were incubated with 20 µg/ml of rituximab in complete R10 medium for 20 min at 37°C and washed three times before adding to eNK cells.

Imaging flow cytometry

YTS-CD16, NK92-CD16, and eNK cells were labeled with CellTrace CFSE. S2-IgG and S2-IC1-IgG cells were labeled with cell proliferation dye eFluor 670. NK cells and target cells were mixed at a 1:2 ratio in 200 µl complete R10 supplemented with anti-CD107a antibody and BD GolgiStop, incubated for 30 min at 37°C, vortexed, and fixed with 1% PFA in PBS. Cell mixtures were run on an Amnis MKII imaging flow cytometer (EMD Millipore), and data were analyzed using IDEAS software (Viswanath et al., 2016).

Anti-S2 polyclonal antibody

Whole S2 cell pellet was used for immunization of rabbits. Rabbit serum was collected after high-dose extension and purified using protein A (custom antibody production; Thermo Fisher Scientific).

Inhibitors

Where applicable, YTS, NK92, and eNK cells were pretreated with 25, 50, or 100 mM ciliobrevin D (EMD Millipore) for 30 min then washed. DMSO was used as the vehicle control for all inhibitor experiments. The inhibitor was also added into the co-culture with target cells.

LFA-1–blocking mAb

For live-cell confocal microscopy, eNK cells were pretreated with 20 µg of anti-CD11a LFA-1 blocking mAb (clone TS1/22) or murine IgG1 mAb (clone MOPC21) for 15 min at 37°C before incubation with the dye-labeled target cells. For standard 4-h ^{51}Cr-cytotoxicity assay, eNK cells were pretreated with IgG or 5, 10, or 20 µg/ml of LFA-1–blocking mAb before incubation with the target cells.

Analysis of synapse geometry

Raw image sequences of YTS-CD16 co-cultured with S2 cells and S2-IgG or S2-IC1-IgG cells were used to characterize the general geometry of the synapse formed between effector and target. In brief, the transmitted light channel was contrasted and smoothed using Gaussian blur tool with a sigma radius of 1 pixel to facilitate the manual outlining of the contours of the cells in ImageJ (version 1.51f). The perimeter of the cells was measured along with the proportion of their respective outline involved in the IS (area of overlapping perimeters between target and effector cells). The total amount of lytic granules in the effector cell was measured as the sum of intensity of the LysoTracker red signal contained within the cell outline in all the focal planes. An axis perpendicular to the synapse was drawn in the effector cell, and the length between the synapse and the opposite side of the cell was measured. The third of the length of this axis, closest from the synapse, was set as the limit of the pool of granules considered as polarized to the synapse. The proportion of the granule at the synapse was then expressed as a ratio of the total signal measured in this area divided by the total amount measured in the cell, both within the limits of the cell outline and in all focal planes acquired.

Image analysis

Raw image sequences were analyzed using Volocity software. For lytic granules, the centroid of individual lytic granule was designated automatically based on the fluorescence intensity of the corresponding staining (LysoTracker red or perforin; Mentlik et al., 2010). For MTOC, in fixed-cell confocal experiments, the point with the highest fluorescence intensity of α-tubulin staining was denoted as the localization of MTOC; in live-cell experiments, the geometric centroid of all the lytic granules in the cell was used to provide a measure of proximity of lytic granule regions. Lytic granule convergence to the MTOC or to the centroid of all granules was measured as previously described (Mentlik et al., 2010). Presentation images were contrast-enhanced uniformly and in general were representative of near mean data from experimental repetitions.

Figure preparation

Fixed-cell confocal images and live-cell image sequences were post-processed in Fiji/ImageJ. Contrast was adjusted using an empirically determined linear transformation, and images were color-merged for display in the figures and supplemental videos. Where applicable, transmitted light and fluorescent channels were smoothed using Gaussian blur tool with a sigma radius of 1 pixel for display purposes. All quantitative analyses were performed on the raw data. For live degranulation images, maximum projection of all *z*-slices in the LysoTracker red and pHluorin channels was used, and only one *z*-slice for the transmitted light channel was used in the display.

Statistical analysis

The minimum number of samples required was determined using sample size calculations based on preliminary data with α and β error levels of 1%. Means of three or more groups were compared using one-way ANOVA, and if significant difference was achieved, individual means were then compared using Student's *t* test. Error bars show ± SD. Differences were considered significant when $P \leq 0.05$ (*, $P < 0.05$; **, $P < 0.01$; ***, $P < 0.001$; ****, $P < 0.0001$).

Online supplemental material

Video 1 shows unconverged lytic granules in a YTS-CD16 cell conjugated with two S2-IgG cells. Video 2 shows converged and polarized lytic granules in YTS-CD16 cells conjugated with two S2-IC1-IgG cells. Video 3 shows that YTS-CD16 cells kill IgG-coated and bystander S2 cells with unconverged lytic granules. Video 4 shows that YTS-CD16 cells kill IgG-coated S2 cells with converged lytic granules. Video 5 shows killing of rituximab-coated Raji cells in the presence of uncoated Raji cells. Video 6 shows killing of rituximab-coated and uncoated Raji cells in the presence of LFA-1 blocking antibody. Fig. S1 shows that LFA-1 but not CD16 engagement induces lytic granule convergence in NK92 cells. Fig. S2 shows that CD16 engagement induces conjugate formation and degranulation in human NK cells. Fig. S3 shows the labeling efficiency and transfer rate of anti–S2-IgG on *Drosophila* S2

cells. Fig. S4 shows the effect of ciliobrevin D on degranulation and the increase of bystander killing by NK cells. Fig. S5 shows no effect of ciliobrevin D on the specific killing rate or viability of human NK cells.

Acknowledgments

The authors acknowledge Drs. Kerry Campbell, John Coligan, and Konrad Krzewski for reagents.

This work was supported by the National Institutes of Health (AI067946 to J.S. Orange).

The authors declare no competing financial interests.

Submitted: 29 April 2016
Revised: 4 September 2016
Accepted: 28 October 2016

References

Banerjee, P.P., R. Pandey, R. Zheng, M.M. Suhoski, L. Monaco-Shawver, and J.S. Orange. 2007. Cdc42-interacting protein-4 functionally links actin and microtubule networks at the cytolytic NK cell immunological synapse. *J. Exp. Med.* 204:2305–2320. http://dx.doi.org/10.1084/jem.20061893

Binyamin, L., R.K. Alpaugh, T.L. Hughes, C.T. Lutz, K.S. Campbell, and L.M. Weiner. 2008. Blocking NK cell inhibitory self-recognition promotes antibody-dependent cellular cytotoxicity in a model of anti-lymphoma therapy. *J. Immunol.* 180:6392–6401. http://dx.doi.org/10.4049/jimmunol.180.9.6392

Blank, C., I. Brown, A.K. Kacha, M.A. Markiewicz, and T.F. Gajewski. 2005. ICAM-1 contributes to but is not essential for tumor antigen cross-priming and CD8+ T cell-mediated tumor rejection in vivo. *J. Immunol.* 174:3416–3420. http://dx.doi.org/10.4049/jimmunol.174.6.3416

Blott, E.J., and G.M. Griffiths. 2002. Secretory lysosomes. *Nat. Rev. Mol. Cell Biol.* 3:122–131. http://dx.doi.org/10.1038/nrm732

Bryceson, Y.T., M.E. March, D.F. Barber, H.G. Ljunggren, and E.O. Long. 2005. Cytolytic granule polarization and degranulation controlled by different receptors in resting NK cells. *J. Exp. Med.* 202:1001–1012. http://dx.doi.org/10.1084/jem.20051143

Christakou, A.E., M. Ohlin, B. Vanherberghen, M.A. Khorshidi, N. Kadri, T. Frisk, M. Wiklund, and B. Önfelt. 2013. Live cell imaging in a micro-array of acoustic traps facilitates quantification of natural killer cell heterogeneity. *Integr Biol (Camb).* 5:712–719. http://dx.doi.org/10.1039/c3ib20253d

Elstak, E.D., M. Neeft, N.T. Nehme, J. Voortman, M. Cheung, M. Goodarzifard, H.C. Gerritsen, P.M. van Bergen En Henegouwen, I. Callebaut, G. de Saint Basile, and P. van der Sluijs. 2011. The munc13-4-rab27 complex is specifically required for tethering secretory lysosomes at the plasma membrane. *Blood.* 118:1570–1578. http://dx.doi.org/10.1182/blood-2011-02-339523

Eriksson, M., G. Leitz, E. Fällman, O. Axner, J.C. Ryan, M.C. Nakamura, and C.L. Sentman. 1999. Inhibitory receptors alter natural killer cell interactions with target cells yet allow simultaneous killing of susceptible targets. *J. Exp. Med.* 190:1005–1012. http://dx.doi.org/10.1084/jem.190.7.1005

Feldmann, J., I. Callebaut, G. Raposo, S. Certain, D. Bacq, C. Dumont, N. Lambert, M. Ouachée-Chardin, G. Chedeville, H. Tamary, et al. 2003. Munc13-4 is essential for cytolytic granules fusion and is mutated in a form of familial hemophagocytic lymphohistiocytosis (FHL3). *Cell.* 115:461–473. http://dx.doi.org/10.1016/S0092-8674(03)00855-9

Fesnak, A.D., C.H. June, and B.L. Levine. 2016. Engineered T cells: The promise and challenges of cancer immunotherapy. *Nat. Rev. Cancer.* 16:566–581. http://dx.doi.org/10.1038/nrc.2016.97

Firestone, A.J., J.S. Weinger, M. Maldonado, K. Barlan, L.D. Langston, M. O'Donnell, V.I. Gelfand, T.M. Kapoor, and J.K. Chen. 2012. Small-molecule inhibitors of the AAA+ ATPase motor cytoplasmic dynein. *Nature.* 484:125–129. http://dx.doi.org/10.1038/nature10936

Gras Navarro, A., A.T. Björklund, and M. Chekenya. 2015. Therapeutic potential and challenges of natural killer cells in treatment of solid tumors. *Front. Immunol.* 6:202. http://dx.doi.org/10.3389/fimmu.2015.00202

Ham, H., W. Huynh, R.A. Schoon, R.D. Vale, and D.D. Billadeau. 2015. HkRP3 is a microtubule-binding protein regulating lytic granule clustering and NK cell killing. *J. Immunol.* 194:3984–3996. http://dx.doi.org/10.4049/jimmunol.1402897

Hamaï, A., F. Meslin, H. Benlalam, A. Jalil, M. Mehrpour, F. Faure, Y. Lecluse, P. Vielh, M.F. Avril, C. Robert, and S. Chouaib. 2008. ICAM-1 has a critical role in the regulation of metastatic melanoma tumor susceptibility to CTL lysis by interfering with PI3K/AKT pathway. *Cancer Res.* 68:9854–9864. http://dx.doi.org/10.1158/0008-5472.CAN-08-0719

Hegde, M., M. Mukherjee, Z. Grada, A. Pignata, D. Landi, S.A. Navai, A. Wakefield, K. Fousek, K. Bielamowicz, K.K. Chow, et al. 2016. Tandem CAR T cells targeting HER2 and IL13Rα2 mitigate tumor antigen escape. *J. Clin. Invest.* 126:3036–3052. http://dx.doi.org/10.1172/JCI83416

Hubbard, A.K., and R. Rothlein. 2000. Intercellular adhesion molecule-1 (ICAM-1) expression and cell signaling cascades. *Free Radic. Biol. Med.* 28:1379–1386. http://dx.doi.org/10.1016/S0891-5849(00)00223-9

Hume, A.N., and M.C. Seabra. 2011. Melanosomes on the move: A model to understand organelle dynamics. *Biochem. Soc. Trans.* 39:1191–1196. http://dx.doi.org/10.1042/BST0391191

Jackson, H.J., S. Rafiq, and R.J. Brentjens. 2016. Driving CAR T-cells forward. *Nat. Rev. Clin. Oncol.* 13:370–383. http://dx.doi.org/10.1038/nrclinonc.2016.36

James, A.M., H.T. Hsu, P. Dongre, G. Uzel, E.M. Mace, P.P. Banerjee, and J.S. Orange. 2013. Rapid activation receptor- or IL-2-induced lytic granule convergence in human natural killer cells requires Src, but not downstream signaling. *Blood.* 121:2627–2637. http://dx.doi.org/10.1182/blood-2012-06-437012

Jones, G.J., J.C. Wiseman, K.J. Marr, S. Wei, J.Y. Djeu, and C.H. Mody. 2009. In contrast to anti-tumor activity, YT cell and primary NK cell cytotoxicity for *Cryptococcus neoformans* bypasses LFA-1. *Int. Immunol.* 21:423–432. http://dx.doi.org/10.1093/intimm/dxp010

Katz, P., A.M. Zaytoun, and J.H. Lee Jr. 1982. Mechanisms of human cell-mediated cytotoxicity. III. Dependence of natural killing on microtubule and microfilament integrity. *J. Immunol.* 129:2816–2825.

Kurowska, M., N. Goudin, N.T. Nehme, M. Court, J. Garin, A. Fischer, G. de Saint Basile, and G. Ménasché. 2012. Terminal transport of lytic granules to the immune synapse is mediated by the kinesin-1/Slp3/Rab27a complex. *Blood.* 119:3879–3889. http://dx.doi.org/10.1182/blood-2011-09-382556

Laan, L., N. Pavin, J. Husson, G. Romet-Lemonne, M. van Duijn, M.P. López, R.D. Vale, F. Jülicher, S.L. Reck-Peterson, and M. Dogterom. 2012. Cortical dynein controls microtubule dynamics to generate pulling forces that position microtubule asters. *Cell.* 148:502–514. http://dx.doi.org/10.1016/j.cell.2012.01.007

Lanier, L.L. 2005. NK cell recognition. *Annu. Rev. Immunol.* 23:225–274. http://dx.doi.org/10.1146/annurev.immunol.23.021704.115526

Liu, D., J.A. Martina, X.S. Wu, J.A. Hammer III, and E.O. Long. 2011. Two modes of lytic granule fusion during degranulation by natural killer cells. *Immunol. Cell Biol.* 89:728–738. http://dx.doi.org/10.1038/icb.2010.167

Lu, C.C., T.S. Wu, Y.J. Hsu, C.J. Chang, C.S. Lin, J.H. Chia, T.L. Wu, T.T. Huang, J. Martel, D.M. Ojcius, et al. 2014. NK cells kill mycobacteria directly by releasing perforin and granulysin. *J. Leukoc. Biol.* 96:1119–1129. http://dx.doi.org/10.1189/jlb.4A0713-363RR

Mace, E.M., P. Dongre, H.T. Hsu, P. Sinha, A.M. James, S.S. Mann, L.R. Forbes, L.B. Watkin, and J.S. Orange. 2014. Cell biological steps and checkpoints in accessing NK cell cytotoxicity. *Immunol. Cell Biol.* 92:245–255. http://dx.doi.org/10.1038/icb.2013.96

March, M.E., C.C. Gross, and E.O. Long. 2010. Use of transfected *Drosophila* S2 cells to study NK cell activation. *Methods Mol. Biol.* 612:67–88. http://dx.doi.org/10.1007/978-1-60761-362-6_6

Marks, M.S., H.F. Heijnen, and G. Raposo. 2013. Lysosome-related organelles: Unusual compartments become mainstream. *Curr. Opin. Cell Biol.* 25:495–505. http://dx.doi.org/10.1016/j.ceb.2013.04.008

Mentlik, A.N., K.B. Sanborn, E.L. Holzbaur, and J.S. Orange. 2010. Rapid lytic granule convergence to the MTOC in natural killer cells is dependent on dynein but not cytolytic commitment. *Mol. Biol. Cell.* 21:2241–2256. http://dx.doi.org/10.1091/mbc.E09-11-0930

Nascimento, A.A., J.T. Roland, and V.I. Gelfand. 2003. Pigment cells: A model for the study of organelle transport. *Annu. Rev. Cell Dev. Biol.* 19:469–491. http://dx.doi.org/10.1146/annurev.cellbio.19.111401.092937

Nilsson, H., M. Rutberg, and M. Wallin. 1996. Localization of kinesin and cytoplasmic dynein in cultured melanophores from Atlantic cod, *Gadus morhua*. *Cell Motil. Cytoskeleton.* 33:183–196. http://dx.doi.org/10.1002/(SICI)1097-0169(1996)33:3<183::AID-CM3>3.0.CO;2-C

Ohlin, M., I. Iranmanesh, A.E. Christakou, and M. Wiklund. 2015. Temperature-controlled MPa-pressure ultrasonic cell manipulation in a microfluidic chip. *Lab Chip.* 15:3341–3349. http://dx.doi.org/10.1039/C5LC00490J

Orange, J.S., S. Roy-Ghanta, E.M. Mace, S. Maru, G.D. Rak, K.B. Sanborn, A. Fasth, R. Saltzman, A. Paisley, L. Monaco-Shawver, et al. 2011. IL-2 induces a WAVE2-dependent pathway for actin reorganization that enables WASp-independent human NK cell function. *J. Clin. Invest.* 121:1535–1548. http://dx.doi.org/10.1172/JCI44862

Peruzzi, G., L. Femnou, A. Gil-Krzewska, F. Borrego, J. Weck, K. Krzewski, and J.E. Coligan. 2013. Membrane-type 6 matrix metalloproteinase regulates the activation-induced downmodulation of CD16 in human primary NK cells. *J. Immunol.* 191:1883–1894. http://dx.doi.org/10.4049/jimmunol.1300313

Rak, G.D., E.M. Mace, P.P. Banerjee, T. Svitkina, and J.S. Orange. 2011. Natural killer cell lytic granule secretion occurs through a pervasive actin network at the immune synapse. *PLoS Biol.* 9:e1001151. http://dx.doi.org/10.1371/journal.pbio.1001151

Ramos, T.N., D.C. Bullard, and S.R. Barnum. 2014. ICAM-1: Isoforms and phenotypes. *J. Immunol.* 192:4469–4474. http://dx.doi.org/10.4049/jimmunol.1400135

Ren, Q., C. Wimmer, M.C. Chicka, S. Ye, Y. Ren, F.M. Hughson, and S.W. Whiteheart. 2010. Munc13-4 is a limiting factor in the pathway required for platelet granule release and hemostasis. *Blood.* 116:869–877. http://dx.doi.org/10.1182/blood-2010-02-270934

Ritter, A.T., Y. Asano, J.C. Stinchcombe, N.M. Dieckmann, B.C. Chen, C. Gawden-Bone, S. van Engelenburg, W. Legant, L. Gao, M.W. Davidson, et al. 2015. Actin depletion initiates events leading to granule secretion at the immunological synapse. *Immunity.* 42:864–876. http://dx.doi.org/10.1016/j.immuni.2015.04.013

Stojanovic, A., and A. Cerwenka. 2011. Natural killer cells and solid tumors. *J. Innate Immun.* 3:355–364. http://dx.doi.org/10.1159/000325465

Viswanath, D.I., E.M. Mace, H.T. Hsu, and J.S. Orange. 2016. Quantification of natural killer cell polarization and visualization of synaptic granule externalization by imaging flow cytometry. *Clin. Immunol.* http://dx.doi.org/10.1016/j.clim.2016.03.004

Vivier, E., E. Tomasello, M. Baratin, T. Walzer, and S. Ugolini. 2008. Functions of natural killer cells. *Nat. Immunol.* 9:503–510. http://dx.doi.org/10.1038/ni1582

Yi, J., X. Wu, A.H. Chung, J.K. Chen, T.M. Kapoor, and J.A. Hammer. 2013. Centrosome repositioning in T cells is biphasic and driven by microtubule end-on capture-shrinkage. *J. Cell Biol.* 202:779–792. http://dx.doi.org/10.1083/jcb.201301004

Zhang, M., M.E. March, W.S. Lane, and E.O. Long. 2014. A signaling network stimulated by β2 integrin promotes the polarization of lytic granules in cytotoxic cells. *Sci. Signal.* 7:ra96. http://dx.doi.org/10.1126/scisignal.2005629

Zografou, S., D. Basagiannis, A. Papafotika, R. Shirakawa, H. Horiuchi, D. Auerbach, M. Fukuda, and S. Christoforidis. 2012. A complete Rab screening reveals novel insights in Weibel-Palade body exocytosis. *J. Cell Sci.* 125:4780–4790. http://dx.doi.org/10.1242/jcs.104174